Estimating Road Angles With the Knowledge of the Vehicle Yaw Angle

Ling-Yuan Hsu
e-mail: lance1214@gmail.com

Tsung-Lin Chen[1]
e-mail: tsunglin@mail.nctu.edu.tw

Department of Mechanical Engineering,
National Chiao Tung University,
Hsinchu,
Taiwan 30010, R.O.C.

This paper presents a method of estimating road angles using state observers and three types of sensors (lateral acceleration sensors, longitudinal velocity sensors, and suspension displacement sensors). The proposed method differs from those in most existing literature in three aspects. First, a "full-state" vehicle model is used to describe nonlinear vehicle dynamics on a sloped road. Second, "switching observer" techniques are used to suggest suitable sensors and to construct state observers. Lastly, the road angles are described by three Euler angles, and two of them are estimated simultaneously. The analysis indicates that (1) road angles affect vehicle dynamics through components of the gravitational force acting on the vehicle body. These gravitational forces can be correctly estimated with an estimation accuracy less than 7.5%, even when road angles vary with time. (2) Those road angles can be correctly estimated only when the vehicle yaw angle is known. [DOI: 10.1115/1.4001330]

1 Introduction

Many research reports have shown that road angles have direct influences on vehicle dynamics, and those effects need to be identified for a satisfactory performance. For example, lacking of road information, rollover prediction systems may produce false alarms [1,2]; vehicle stability controls may either initiate false activation or need large actuation power [3,4]. The road angle problems are difficult to tackle with because it is neither practical to assume that road angles can be obtained beforehand, nor measure them in real time using sensors attached to a vehicle body. Road angles are difficult to measure in real time because they are often coupled with other vehicle dynamics in sensor measurements, such as vehicle roll/pitch angles, lateral accelerations, etc. [5–8].

In general, road angles are described by the "road curve angle," "road bank angle," and "road grade angle," as shown in Fig. 1. Even though the road bank/grade angle and the vehicle roll/pitch angle have indistinguishable influences on sensor measurements, they play very different roles in vehicle dynamics. Therefore, some researchers proposed using vehicle dynamics and state observer techniques to estimate road angles [3,7,9]. In order to achieve a reliable estimation of road angles with less amount of sensor deployments, the incorporated vehicle model must be as precise as possible; this leads to high-order, nonlinear differential equations for vehicle modeling. Some conventional nonlinear observer design methods, such as the extended Kalman filter (EKF), require information from the Jacobian matrices of system equations and measurement equations at each sampling time [10]. To construct such an observer for an n-state, m-output nonlinear system, one needs to derive/code $(n \times n + m \times n)$ equations by hand. For high-order nonlinear vehicle systems, this is impractical. Partly for that reason, most road angle estimation systems employ more amounts of sensors to work with simplified vehicle models [3,7–9,11].

In most road angle estimation literature, the coordinate systems were defined in a way that the road curve angle was aligned with the vehicle yaw angle. And the estimations were performed on either road bank angle [4,3,6,8] or road grade angle [9,12]; only a few on those two angles simultaneously [7,5,11]. And, in those two-angle estimations, the road bank angle and grade angle were both referred to the same coordinate, which is totally different from the conventional "Euler angle" approach [13]. Consequently, even one knows the heading direction of a vehicle (vehicle yaw angle), it is still difficult to picture (calculate) the road terrain from the values of their road bank angle and road grade angle.

Previously, the author proposed a novel switching computation scheme [2], which can solve differential equations numerically. With that method, a set of high-order differential equations is separated into two sets of low-order differential equations. These two sets of low-order differential equations calculate state values in a way similar to "domain decomposition methods [14]." The state values obtained from this method can be fairly close to those of the analytical solutions. The analysis of stability and convergence [1] indicates that, by choosing a proper "switching time," the computation accuracy is proportional to the switching time to the power of 2. This method can be extended to the state observer construction for high-order nonlinear systems with the benefit of reducing a large amount of equation derivations.

In this paper, we present a novel approach to estimate road bank angle, road grade angle, and their effects on vehicle dynamics. In this method, estimating road angles needs the information of vehicle yaw angle but estimating the road angle effects does not. Unlike other approaches in this aspect, the conventional Euler angle is used to describe a road terrain, and the referenced coordinate system is fixed on Earth. Thus, the description of terrain is intuitive and independent of the vehicle yaw angle. Since the estimation of road angles is achieved by the angle influence on vehicle dynamics, a "full-state" vehicle model (22 states, nonlinear differential equations) is incorporated to ensure the estimation accuracy under various vehicle maneuvers. As discussed before, using such a high-order nonlinear model in state estimations would require lots of equation derivations. Therefore, the previously proposed switching computation techniques are used to suggest suitable sensors and to reduce the amount of equation derivations. The procedures of constructing the estimation system and the observability analysis of road angle estimations are both discussed in detail in this paper.

2 Vehicle Model

2.1 Coordinate Systems and Euler Angles. Two sets of Euler angles and four coordinate systems shown in Fig. 2 are intro-

[1]Corresponding author.

Contributed by the Dynamic Systems Division of ASME for publication in the JOURNAL OF DYNAMIC SYSTEMS, MEASUREMENT, AND CONTROL. Manuscript received October 29, 2008; final manuscript received December 10, 2009; published online April 14, 2010. Assoc. Editor: J. Karl Hedrick.

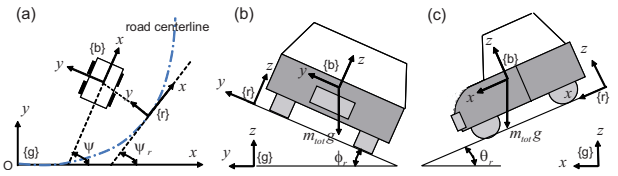

Fig. 1 A vehicle on a sloped road: (*a*) the road curve angle ψ_r, (*b*) the road bank angle ϕ_r, and (*c*) the road grade angle θ_r

duced for constructing the vehicle model. These four coordinate systems are global frame {g}, road frame {r}, body frame {b}, and auxiliary frame {a}. Similar to conventional approaches, the global frame is fixed to a point on Earth, whereas the body frame is fixed to the center of gravity (CG) of the vehicle. In addition to conventional approaches, the road frame is introduced to describe vehicle dynamics on a sloped road. The relationship between the road frame and the global frame is described by the Euler angles $(\theta_r, \phi_r, \psi_r)$, which are referred to as the road grade angle, road bank angle, and road curve angle, respectively. The relationship between the road frame and the body frame is described by another set of Euler angles (ψ, θ, ϕ). These three angles describe the vehicle attitude relative to the road level and are referred to as the "vehicle yaw angle," "vehicle pitch angle," and "vehicle roll angle," respectively. Since the vehicle may move along a path irrelevant to road curve angles, the road curve angle does not affect the vehicle dynamics. Thus, it is assumed to be zero ($\psi_r = 0$) in this paper.

The auxiliary frame (aux-frame) is obtained by rotating the z-axis of the road frame until the x-axis of the road frame is aligned with the x-axis of the body frame. The aux-frame is used because it describes the vehicle translational motions in an intuitive manner while preserving the information of other vehicle dynamics relative to the road level. In the following vehicle modeling, vehicle translational motions are described in the aux-frame, and the rotational motions are described by Euler angles (ψ, θ, ϕ).

2.2 Road Angle Effects and Vehicle Modeling. As shown in Fig. 1, Earth's gravity is an external force acting on the vehicle body and is fixed to the global frame. Therefore, it affects vehicle dynamics via road angles. If the sloped road is described by the Euler angles $(\theta_r, \phi_r, \psi_r)$ with the rotation order of "pitch-roll-yaw" and the road curve angle is zero ($\psi_r = 0$), three components of the gravitational force, presented in the aux-frame (G_x^a, G_y^a, G_z^a), can be obtained as

$$\begin{bmatrix} G_x^a \\ G_y^a \\ G_z^a \end{bmatrix} = \begin{bmatrix} \cos\psi & \sin\psi & 0 \\ -\sin\psi & \cos\psi & 0 \\ 0 & 0 & 1 \end{bmatrix} \begin{bmatrix} 1 & 0 & 0 \\ 0 & \cos\phi_r & \sin\phi_r \\ 0 & -\sin\phi_r & \cos\phi_r \end{bmatrix} \times \begin{bmatrix} \cos\theta_r & 0 & -\sin\theta_r \\ 0 & 1 & 0 \\ \sin\theta_r & 0 & \cos\theta_r \end{bmatrix} \begin{bmatrix} 0 \\ 0 \\ -g \end{bmatrix} \quad (1)$$

where g is Earth's gravity. Since Earth's gravity is the only external force that is fixed to the global frame in most cases, the "road angle effects" on vehicle dynamics can be attributed to these gravitational forces (G_x^a, G_y^a, G_z^a).

Similar to other researches [15,16], the vehicle modeling is proceeded with the "sprung mass system" and "unsprung mass system." Assuming that the vehicle body is rigid, the dynamics of the sprung mass system, presented in the aux-frame, is

$$m_{\text{tot}}(\ddot{x}^a - \dot{y}^a\dot{\psi}) = \sum F_{x,\text{tire}}^a + m_{\text{tot}}G_x^a$$

$$m_{\text{tot}}(\ddot{y}^a + \dot{x}^a\dot{\psi}) = \sum F_{y,\text{tire}}^a + m_{\text{tot}}G_y^a$$

$$m_{\text{tot}}\ddot{z}^a = \sum F_{z,\text{spring}}^a + m_{\text{tot}}G_z^a$$

$$\ddot{\phi} = \ddot{\psi}\sin\theta + \dot{\psi}\dot{\theta}\cos\theta + \bar{M}_x$$

$$\ddot{\theta} = -\dot{\psi}\dot{\phi}\cos\theta + \bar{M}_y\cos\phi - \bar{M}_z\sin\phi$$

$$\ddot{\psi} = \dot{\theta}\dot{\phi}\sec\theta + \dot{\psi}\dot{\theta}\tan\theta + \bar{M}_y\sin\phi\sec\theta + \bar{M}_z\cos\phi\sec\theta$$

$$\bar{M}_x = \frac{M_x}{I_x} - \frac{I_z - I_y}{I_x}(\dot{\theta}\cos\phi + \dot{\psi}\cos\theta\sin\phi)(-\dot{\theta}\sin\phi + \dot{\psi}\cos\theta\cos\phi)$$

$$\bar{M}_y = \frac{M_y}{I_y} - \frac{I_x - I_z}{I_y}(\dot{\phi} - \dot{\psi}\sin\theta)(-\dot{\theta}\sin\phi + \dot{\psi}\cos\theta\cos\phi)$$

$$\bar{M}_z = \frac{M_z}{I_z} - \frac{I_y - I_x}{I_z}(\dot{\phi} - \dot{\psi}\sin\theta)(\dot{\theta}\cos\phi + \dot{\psi}\cos\theta\sin\phi) \quad (2)$$

where the superscript a indicates state values represented in the aux-frame; x^a, y^a, and z^a are the translational displacements of the vehicle CG; $F_{x,\text{tire}}^a$, $F_{y,\text{tire}}^a$, and $F_{z,\text{spring}}^a$ are the translational forces

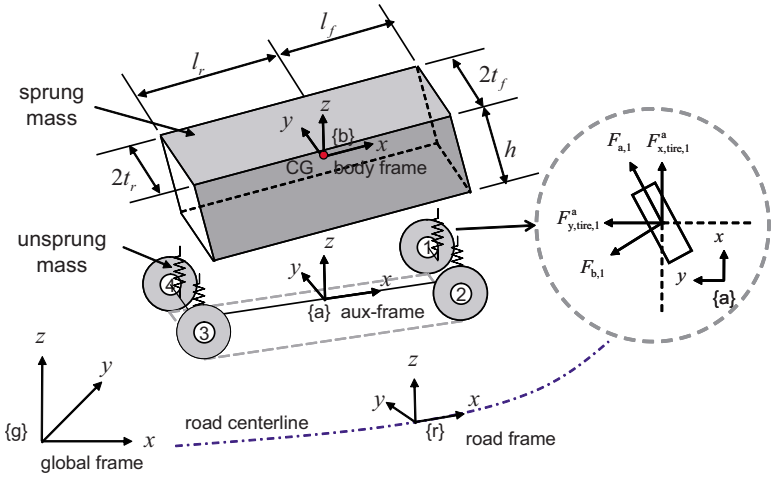

Fig. 2 Four coordinate systems for the vehicle modeling. {g}: global frame, {b}: body frame, {r}: road frame, and {a}: aux-frame.

generated by tires and suspension systems; M_x, M_y, and M_z are the external torques acting on the vehicle CG along three axes of the body frame; and I_x, I_y, and I_z are the moments of inertia of the sprung mass system along three axes of the body frame. The dynamics of the unsprung mass system, presented in the aux-frame, is

$$I_{w,i}\dot{\omega}_i^a = -r_{e,i}F_{a,i} - T_{b,i} + T_{m,i} \quad (i = 1-4)$$

$$\dot{H}_1^a = -\dot{z}^a + l_f\dot{\theta}\cos\theta + t_f(\dot{\theta}\sin\theta\sin\phi - \dot{\phi}\cos\theta\cos\phi)$$

$$\dot{H}_2^a = -\dot{z}^a + l_f\dot{\theta}\cos\theta - t_f(\dot{\theta}\sin\theta\sin\phi - \dot{\phi}\cos\theta\cos\phi)$$

$$\dot{H}_3^a = -\dot{z}^a - l_r\dot{\theta}\cos\theta - t_r(\dot{\theta}\sin\theta\sin\phi - \dot{\phi}\cos\theta\cos\phi)$$

$$\dot{H}_4^a = -\dot{z}^a - l_r\dot{\theta}\cos\theta + t_r(\dot{\theta}\sin\theta\sin\phi - \dot{\phi}\cos\theta\cos\phi) \quad (3)$$

where ω_i^a represents the angular rate of each tire i; $F_{a,i}$ is the longitudinal adhesive force generated by tire i; $T_{b,i}$ and $T_{m,i}$ are the braking and traction torque transmitted to tire i, respectively; $I_{w,i}$ is the moment of inertia of tire i; $r_{e,i}$ is the effective rolling radius of tire i; H_i^a represents the displacement of each suspension corner i; the subscript i refers to four suspension corners in a way: $1 \rightarrow$ front-left, 2 to 4 in a clockwise motion; l_f and l_r are the distances from the CG to the front and rear axes, respectively; and t_f and t_r are one-half the distances of the front and rear tracks, respectively. More details of this vehicle modeling can be found in Refs. [1,2].

3 Road Angle Estimations

In this paper, two road angles (θ_r, ϕ_r) are treated as system states and identified by state observer techniques. In order to apply existing observer algorithms to this problem, the "dynamic equations" of road angles should be obtained prior to the observer construction. However, it is neither practical to use sensors, attached to a vehicle body, to measure the change rate of road angles, nor to obtain this information for a specific road terrain. The change rates of these two angles are assumed to be zeros for now (Eq. (4)). Although this assumption leads to model errors when the vehicle is moving on a road with varying road angles, this error can be alleviated using some robust observer designs, which will be discussed shortly.

$$\dot{\theta}_r = 0$$

$$\dot{\phi}_r = 0 \quad (4)$$

From Eqs. (1)–(4), one can obtain a 22-state vehicle model that can mimic vehicle behaviors on a sloped road. This vehicle model is used to construct the state observer for estimating road angles and their effects.

3.1 Switching Observer Scheme. As discussed before, using the conventional EKF to construct an observer for a 22-state nonlinear system, one must derive 484 partial derivative terms ($22 \times 22 = 484$). Moreover, to examine the feasibility of a sensor candidate, one must derive at least 22 derivative terms. It is difficult to do so. The switching observer scheme [2], developed from a switching computation scheme, is used to suggest suitable sensors and reduce the intensive equation derivations. In that case, one can then design two individual observers; one observer requires 144 partial derivative terms while the other requires 100 partial derivative terms. The amount of derivations is roughly one-half of that required for the conventional EKF. As shown in Fig. 3, the switching observer scheme is operated in a way that, within each switching cycle, one observer estimates state values while the other observer is held static. They switch their roles in the next switching cycle.

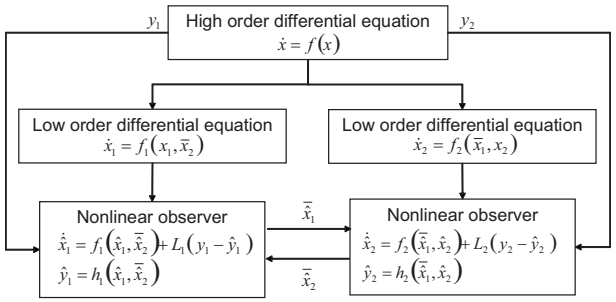

Fig. 3 A diagram of the switching observer scheme. One observer estimates state values within a switching cycle while the other is held static. They switch their roles of estimating state values in the next cycle.

3.2 Vehicle Yaw Model and Vehicle Roll Model. Following the concepts of switching computation scheme, this 22-state vehicle model is separated into a 12-state submodel ($[\dot{\psi}, \psi, \dot{x}^a, x^a, \dot{y}^a, y^a, \omega_{1-4}^a, \theta_r, \phi_r]^T$) and a 10-state submodel ($[\dot{\phi}, \phi, \dot{\theta}, \theta, \dot{z}^a, z^a, H_{1-4}^a]^T$). They are referred to as the vehicle yaw model and vehicle roll model in this paper.

Vehicle yaw model:

$$\ddot{\psi} = \dot{\theta}\dot{\phi}\sec\theta + \dot{\psi}\dot{\theta}\tan\theta + \bar{M}_y\sin\phi\sec\theta + \bar{M}_z\cos\phi\sec\theta$$

$$\dot{x}^a = \dot{y}^a\dot{\psi} + \sum F_{x,\text{tire}}^a/m_{\text{tot}} + G_x^a$$

$$\dot{y}^a = -\dot{x}^a\dot{\psi} + \sum F_{y,\text{tire}}^a/m_{\text{tot}} + G_y^a$$

$$I_{w,i}\dot{\omega}_i^a = -r_{e,i}F_{a,i} - T_{b,i} + T_{m,i}$$

$$\dot{\theta}_r = 0$$

$$\dot{\phi}_r = 0 \quad (5)$$

Vehicle roll model:

$$\ddot{\phi} = \ddot{\psi}\sin\theta + \dot{\psi}\,\dot{\theta}\cos\theta + \bar{M}_x$$

$$\ddot{\theta} = -\dot{\psi}\dot{\phi}\cos\theta + \bar{M}_y\cos\phi - \bar{M}_z\sin\phi$$

$$\ddot{z}^a = \sum F_{z,\text{spring}}^a/m_{\text{tot}} + G_z^a$$

$$\dot{H}_1^a = -\dot{z}^a + l_f\dot{\theta}\cos\theta + t_f(\dot{\theta}\sin\theta\sin\phi - \dot{\phi}\cos\theta\cos\phi)$$

$$\dot{H}_2^a = -\dot{z}^a + l_f\dot{\theta}\cos\theta - t_f(\dot{\theta}\sin\theta\sin\phi - \dot{\phi}\cos\theta\cos\phi)$$

$$\dot{H}_3^a = -\dot{z}^a - l_r\dot{\theta}\cos\theta - t_r(\dot{\theta}\sin\theta\sin\phi - \dot{\phi}\cos\theta\cos\phi)$$

$$\dot{H}_4^a = -\dot{z}^a - l_r\dot{\theta}\cos\theta + t_r(\dot{\theta}\sin\theta\sin\phi - \dot{\phi}\cos\theta\cos\phi) \quad (6)$$

According to Eqs. (1) and (2), road angles have a direct impact on three translational accelerations. For the accuracy of state estimation, the "dynamics" of two road angles reside in the vehicle yaw model because the vehicle yaw model contains more translational dynamics than the vehicle roll model.

Note that this is not the only way of splitting a vehicle system. From the stability analysis of the switching computation scheme, the system (states) splitting can be done differently as long as it satisfies certain stability constraints [1].

3.3 Sensor Selection. According to Eq. (2), the road angle affects vehicle dynamics in many aspects. Therefore, in order to correctly estimate road angles from vehicle dynamics, most vehicle states must be known or correctly estimated. For this reason,

sensors are chosen to ensure that most of the 22 vehicle states are observable. Here, we choose lateral acceleration sensors, longitudinal velocity sensors, and four suspension displacement sensors for this estimation system. Although longitudinal velocity sensors are not popular in commercial vehicles, a global positioning system (GPS)/inertial navigation system (INS) sensor system can provide the information of the longitudinal velocity [17,18]. However, the output of the GPS/INS systems needs lots of signal processing to obtain the velocity information, and is beyond the scope of this paper. We assume that the longitudinal velocity sensor is available for simplicity.

When adapting the switching observer scheme, the lateral acceleration sensors and longitudinal velocity sensors ($\mathbf{Y}_1$ in Eq. (7)) work with the state observer of the vehicle yaw model, while the four suspension displacement sensors ($\mathbf{Y}_2$ in Eq. (8)) work with the state observer of vehicle roll model.

$$\mathbf{Y}_1 = \begin{bmatrix} \ddot{y}_m^g \\ \dot{x}_m^a \end{bmatrix} = \begin{bmatrix} (\ddot{x}^a - \dot{y}^a\dot{\psi} + G_x^a)\sin\phi\sin\theta + (\ddot{y}^a + \dot{x}^a\dot{\psi} + G_y^a)\cos\phi + (\ddot{z}^a + G_z^a)\sin\phi\cos\theta \\ \dot{x}^a \end{bmatrix} \tag{7}$$

$$\mathbf{Y}_2 = \begin{bmatrix} H_{1,m}^a \\ H_{2,m}^a \\ H_{3,m}^a \\ H_{4,m}^a \\ H_{1,m}^a \\ H_{2,m}^a \\ H_{3,m}^a \\ H_{4,m}^a \end{bmatrix} = \begin{bmatrix} H_1^a \\ H_2^a \\ H_3^a \\ H_4^a \\ -z^a + l_f\sin\theta - t_f\cos\theta\sin\phi \\ -z^a + l_f\sin\theta + t_f\cos\theta\sin\phi \\ -z^a - l_r\sin\theta + t_r\cos\theta\sin\phi \\ -z^a - l_r\sin\theta - t_r\cos\theta\sin\phi \end{bmatrix} \tag{8}$$

Note that there are duplicated output equations in $\mathbf{Y}_2$ and they share the same values from corresponding sensor measurements $H_{i,m}^a$. This is because the suspension displacement H_i^a is either a redundant or independent state depending on whether the tire i is on or off the ground [2]. Once a tire is identified to be off the ground, its duplicated equation is removed as it is no longer valid. For example, if the first tire is identified to be off the ground, the fifth equation in $\mathbf{Y}_2$ is removed. These duplicated equations ensure the success of state estimation no matter tires are on or off the ground.

3.4 Observer Algorithm. The observer algorithms are chosen to be the EKF because it is simple and effective in the sensor noise reduction. Although the EKF has been questioned for the state convergence [10]; in that case, one can use the iterative Kalman filter (IKF) to obtain both noise reduction and state convergence.

As discussed before, the assumption of constant road angles (Eq. (4)) may lead to modeling error for state estimations. Normally, the model error can be dealt with by two methods in Kalman filtering: One adds large fictitious noise to dynamic equations [10], and the other one uses robust observer design such as "fading memory techniques [19,20]." The fading memory technique is done by introducing a "forgetting factor" into the computation of the "predicted covariance matrix" in EKF [10]. The predicted covariance matrix is then increased; thus the observer would believe more in sensor outputs than in system models. The forgetting factor can be chosen in a way that optimizes the performance of state convergence and noise reduction [19,20]. However, the equation derivation is beyond the scope of this paper and thus omitted. Hence, the EKF accompanied with fading memory techniques is utilized in this paper.

4 Observability Analysis

The success of state estimations depends on the system observability. And the local observability of a nonlinear system is determined by the rank of the observability matrix, which is comprised of partial derivatives of the measurement equations and their derivatives [21]. In this vehicle system, the observability matrix can be written as

$$\mathbf{W}_o \equiv \nabla\left[\begin{bmatrix}\mathbf{Y}_1\\ \mathbf{Y}_2\end{bmatrix}, \begin{bmatrix}\dot{\mathbf{Y}}_1\\ \dot{\mathbf{Y}}_2\end{bmatrix}, \begin{bmatrix}\ddot{\mathbf{Y}}_1\\ \ddot{\mathbf{Y}}_2\end{bmatrix}, \cdots\right]^T \tag{9}$$

As discussed before, this estimation system is designed to ensure most of vehicle states converging to their correct values. For better understanding of the system observability, the observability analysis is proceeded for road angles first and then for the entire vehicle states.

4.1 Observability Analysis for Road Angles. The road angles (θ_r, ϕ_r) affect vehicle dynamics only through three gravitational forces (G_x^a, G_y^a, G_z^a). Thus, these gravitational forces must be observable for the possible observability of road angles. Therefore, the observability of gravitational forces is examined first. With those selected sensors, the observability of gravitational forces can be determined by the following matrix:

$$\mathbf{W}_{o,\text{gravity}} = \frac{\partial}{\partial \mathbf{G}^a}\left[\begin{bmatrix}\mathbf{Y}_1\\ \mathbf{Y}_2\end{bmatrix}, \begin{bmatrix}\dot{\mathbf{Y}}_1\\ \dot{\mathbf{Y}}_2\end{bmatrix}, \begin{bmatrix}\ddot{\mathbf{Y}}_1\\ \ddot{\mathbf{Y}}_2\end{bmatrix}\right]^T$$

$$= \begin{bmatrix} 2\sin\phi\sin\theta & 2\cos\phi & 2\sin\phi\cos\theta \\ 0 & 0 & 0 \\ \mathbf{0}_{8\times1} & \mathbf{0}_{8\times1} & \mathbf{0}_{8\times1} \\ \dfrac{\partial\ddot{y}_m^g}{\partial\dot{x}^a} & \dfrac{\partial\ddot{y}_m^g}{\partial\dot{y}^a} & \dfrac{\partial\ddot{y}_m^g}{\partial\dot{z}^a} \\ 1 & 0 & 0 \\ \mathbf{0}_{8\times1} & \mathbf{0}_{8\times1} & \mathbf{0}_{8\times1} \\ \left(\dfrac{\partial\ddot{x}^a}{\partial\dot{x}^a} + \dfrac{\partial\ddot{y}^a}{\partial\dot{x}^a}\right)\dfrac{\partial\ddot{y}_m^g}{\partial\dot{x}^a} & \left(\dfrac{\partial\ddot{x}^a}{\partial\dot{y}^a} + \dfrac{\partial\ddot{y}^a}{\partial\dot{y}^a}\right)\dfrac{\partial\ddot{y}_m^g}{\partial\dot{y}^a} & \left(\dfrac{\partial\ddot{z}^a}{\partial\dot{z}^a} + 1\right)\dfrac{\partial\ddot{y}_m^g}{\partial\dot{z}^a} \\ 0 & 0 & 0 \\ \mathbf{0}_{8\times1} & \mathbf{0}_{8\times1} & \mathbf{1}_{8\times1} \end{bmatrix}$$

$$\mathbf{G}^a = \begin{bmatrix} G_x^a, & G_y^a, & G_z^a \end{bmatrix}^T \tag{10}$$

The rank of the above matrix can be 3 but it depends on the state values of other vehicle dynamics. Meaning that if those vehicle states can be measured or correctly estimated, three gravitational forces can be correctly estimated.

The observability of three angles (θ_r, ϕ_r, ψ) that parametrized gravitational forces in Eq. (1) can be calculated by "chain-rules" techniques

$$\mathbf{W}_{o,\text{angle}} = \frac{\partial}{\partial\{\theta_r,\phi_r,\psi\}}\left[\begin{bmatrix}\mathbf{Y}_1\\ \mathbf{Y}_2\end{bmatrix}, \begin{bmatrix}\dot{\mathbf{Y}}_1\\ \dot{\mathbf{Y}}_2\end{bmatrix}, \begin{bmatrix}\ddot{\mathbf{Y}}_1\\ \ddot{\mathbf{Y}}_2\end{bmatrix}, \cdots\right]^T = \frac{\partial}{\partial\{\mathbf{G}^a,\dot{\mathbf{G}}^a,\cdots\}}\left[\begin{bmatrix}\mathbf{Y}_1\\ \mathbf{Y}_2\end{bmatrix}, \begin{bmatrix}\dot{\mathbf{Y}}_1\\ \dot{\mathbf{Y}}_2\end{bmatrix}, \begin{bmatrix}\ddot{\mathbf{Y}}_1\\ \ddot{\mathbf{Y}}_2\end{bmatrix}, \cdots\right]^T \cdot \mathbf{G}$$

$$\mathbf{G} \equiv \frac{\partial}{\partial\{\theta_r,\phi_r,\psi\}}\left[\mathbf{G}^a, \ \dot{\mathbf{G}}^a, \ \cdots\right]^T$$

Since three gravitational forces are observable mostly, the rank of $\mathbf{W}_{o,\text{angle}}$ can be determined by the rank of $\mathbf{G}$ matrix only. By ignoring those derivative terms $[\dot{\mathbf{G}}^a,\cdots]$ in $\mathbf{G}$ matrix for now, the rank of the matrix can be determined by the following:

$$\frac{\partial \mathbf{G}^a}{\partial\{\theta_r,\phi_r,\psi\}} = \begin{bmatrix} -g(-\cos\theta_r\cos\psi\cdots-\sin\theta_r\sin\phi_r\sin\psi) & -g(\cos\theta_r\cos\phi_r\sin\psi) & -g(\sin\theta_r\sin\psi\cdots+\cos\theta_r\sin\phi_r\cos\psi)\\ -g(\cos\theta_r\sin\psi\cdots-\sin\theta_r\sin\phi_r\cos\psi) & -g(\cos\theta_r\cos\phi_r\cos\psi) & -g(\sin\theta_r\cos\psi\cdots-\cos\theta_r\sin\phi_r\sin\psi)\\ -g(-\sin\theta_r\cos\phi_r) & -g(-\cos\theta_r\sin\phi_r) & 0 \end{bmatrix} \tag{11}$$

It can be shown that the above matrix is unconditionally singular and its rank is 2. In that case, according to Ref. [22], including more derivative terms ($[\dot{\mathbf{G}}^a,\cdots]$) would not increase the rank of the observability matrix $\mathbf{G}$.

4.2 Observability Analysis for Vehicle Dynamics. The observability of the overall vehicle system (22 states) is examined to show if those state values can be correctly obtained. Because of the switching observer scheme, the observability is checked for the vehicle yaw model and vehicle roll model separately.

4.2.1 Vehicle Yaw Model. Before examining the rank of the observability matrix of the vehicle yaw model, we first check the partial derivatives of the measurement equations ($\mathbf{Y}_1$) and its derivatives with respect to the states of longitudinal displacement (x^a) and lateral displacement (y^a).

$$\frac{\partial}{\partial x^a}\begin{bmatrix}\mathbf{Y}_1\\ \dot{\mathbf{Y}}_1\\ \vdots\end{bmatrix} = \frac{\partial}{\partial y^a}\begin{bmatrix}\mathbf{Y}_1\\ \dot{\mathbf{Y}}_1\\ \vdots\end{bmatrix} = \begin{bmatrix}0\\ 0\\ \vdots\end{bmatrix}_{n\times 1} \tag{12}$$

Equation (12) reveals that the associated partial derivatives are all zeros, and thus the longitudinal displacement and lateral displacement are globally unobservable. This result can be understood by the fact that displacement information cannot be obtained by neither acceleration sensors nor velocity sensors.

The rank of the observability matrix of the vehicle yaw model is difficult to calculate analytically because it requires lots of equation derivations. In this case, a trajectory of the vehicle states is specified and the rank of the observability matrix is calculated numerically. The simulation results show that the rank of the observability matrix is 9. Since (i) all the elements in Eq. (12) are zeros, (ii) three gravitational forces are observable (Eq. (10)), and (iii) the observability matrix of three angles (θ_r,ϕ_r,ψ) loses one rank (Eq. (11)), one can conclude that, except the longitudinal displacement, lateral displacement, and one angle from (θ_r,ϕ_r,ψ), the rest of states in the vehicle yaw model are all observable along this special trajectory.

4.2.2 Vehicle Roll Model. For simplicity, we check the observability of the vehicle roll model using measurement equations $\mathbf{Y}_2$ and their first derivatives only, which leads to the following:

$$\mathbf{W}_{o,\text{roll}} = \nabla\begin{bmatrix}\mathbf{Y}_2\\ \dot{\mathbf{Y}}_2\end{bmatrix} = \begin{bmatrix}\mathbf{0}_{4\times 6} & \mathbf{I}_{4\times 4}\\ \mathbf{A}_{12\times 6} & \mathbf{0}_{12\times 4}\end{bmatrix}_{16\times 10} \tag{13}$$

where $\mathbf{I}$ is an identity matrix. One can prove that the rank of the lower-left matrix $\mathbf{A}$ is 6, except at θ=90 deg. Thus, all states in the vehicle roll model are observable except when the vehicle pitch angle is 90 deg. Furthermore, the derivation indicates that the rank of the observability matrix can still be 10 when two of the duplicated measurement equations in Eq. (8) are removed from the observability matrix. This finding suggests that two of those duplicated measurement equations are redundant for state estimation. However, since it is impossible to know in advance which tire would lift off, all four duplicated measurement equations are used.

Since the vehicle states appearing in $\mathbf{W}_{o,\text{gravity}}$ are all observable and the $\mathbf{W}_{o,\text{gravity}}$ matrix is nonsingular, it is possible to choose a suitable observer algorithm to correctly estimate three gravitational forces. On the other hand, since the rank of the observability matrix $\mathbf{W}_{o,\text{angle}}$ is 2, those three angles (θ_r,ϕ_r,ψ) can be correctly estimated only when one of them is known.

5 Numerical Simulation

The following simulations are meant to validate the feasibility of the proposed method. In these simulations, the vehicle moves at an initial longitudinal speed of 25 m/s and then the steering wheel makes a left-hand turn, as shown in Fig. 4. For simplicity, the noises associated with all the integrated sensors (lateral acceleration sensor, longitudinal velocity sensor, and suspension displacement sensors) are assumed to be white, and their standard deviations are 0.08 m/s^2, 0.01 m/s, and 0.01 m, respectively. Simulation results are shown in Figs. 5–11. The state values from

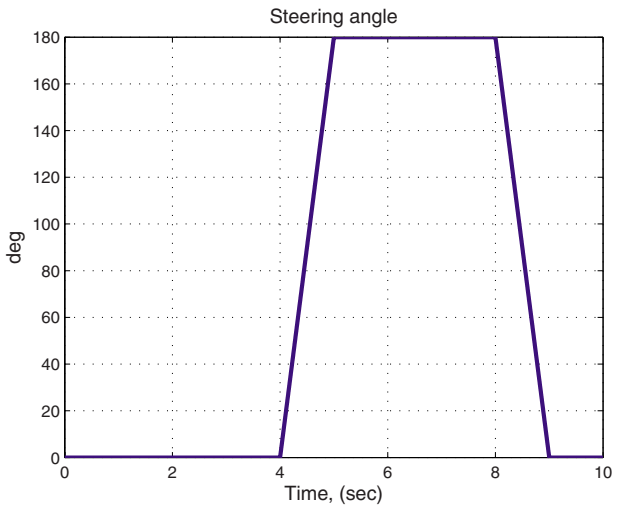

Fig. 4 Vehicle maneuvering: steering angle versus time

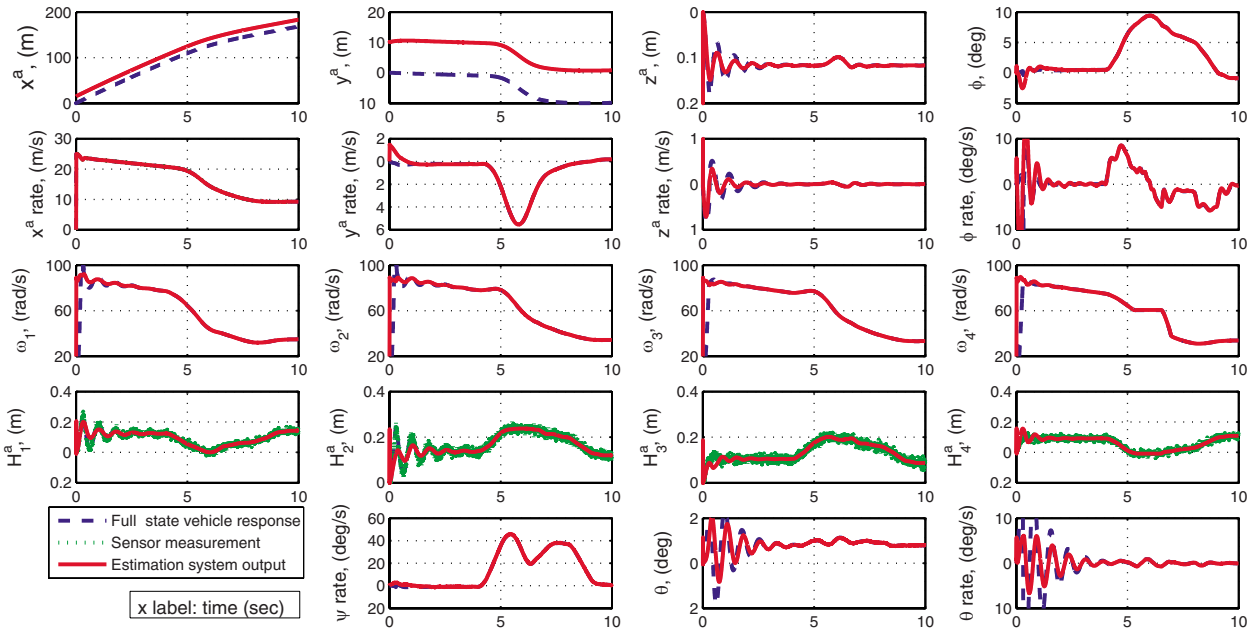

Fig. 5 Estimating vehicle dynamics for Case I. The estimation system can estimate most vehicle dynamics correctly, except for longitudinal displacement x^a and lateral displacement y^a.

the full-state vehicle model are shown in dashed-blue lines and represent real vehicle dynamics. The state values from the sensor output equation are shown in dotted-green lines and represent real sensor measurement. The state values from the proposed estimation system are shown in solid-red lines. Both the sampling time of the system and the switching time of the switching observers are set at 0.001 s.

Case I shows a vehicle moving on a road with the road bank angle of 5 deg and road grade angle of −5 deg. As shown in Fig. 5, the estimation system can estimate most vehicle dynamics correctly, except for the longitudinal displacement (x^a) and lateral displacement (y^a). Also, as shown in Fig. 6, the estimation system can estimate three gravitational forces correctly but fails to estimate three angles (θ_r, ϕ_r, ψ). These simulation results agree very well with the analysis shown in Sec. 4.

These results can be further verified by the singular values of the corresponding observability matrix. The observability matrices of gravitational force ($\mathbf{W}_{o,\text{gravity}}$) and of angle estimations ($\mathbf{W}_{o,\text{angle}}$) are calculated at each sampling time, and their corresponding singular values are drawn in Fig. 7. All singular values are nonzero for the gravitational forces, and thus the estimations of these forces are correct. On the other hand, because one of the singular values for road angles is zero, the estimations of those angles are erroneous. Furthermore, the relative accuracy (≡(estimated value−real value)/(real value) [23]) of the gravitational force estimation is on average of 0.22%, 0.14%, and 0.006% for G_x^a, G_y^a, and G_z^a, respectively.

Case II shows a vehicle moving on a road. The conditions in this case are the same as those in Case I, except that the sensor system provides additional measurements: vehicle yaw angle with a standard deviation of 0.01 rad. As shown in Fig. 8, the estimation system can estimate accurately for three gravitational forces as well as for three angles (θ_r, ϕ_r, ψ). This simulation results agree with the arguments shown in Sec. 4. The relative accuracies of state estimations are 0.48%, 0.64%, and 0.55% for θ_r, ϕ_r, and ψ, and 0.82%, 0.42%, and 0.003% for G_x^a, G_y^a, and G_z^a.

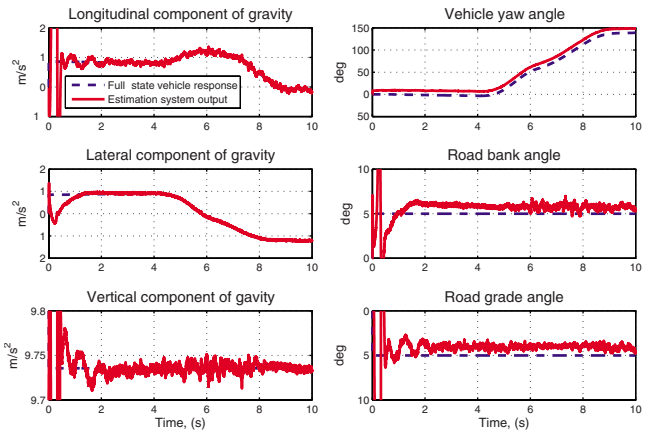

Fig. 6 Estimating road angles and their effects for Case I. The estimation system can estimate three gravitational forces accurately but fails to estimate three angles.

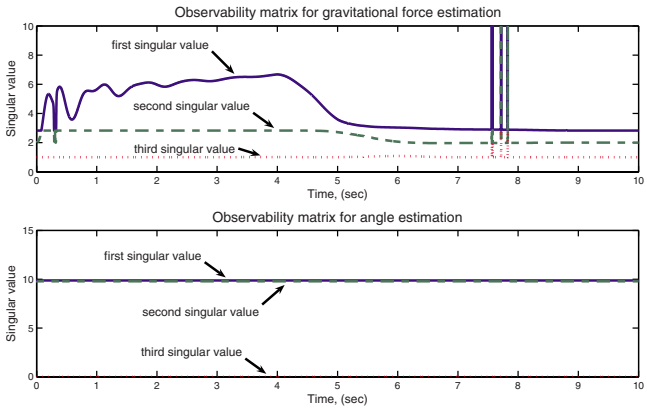

Fig. 7 Singular values of the observability matrices for gravitational force estimations and for angle estimations. None of the singular value of the gravitational force estimation is zero. One of the singular values of the angle estimation is zero along the entire trajectory.

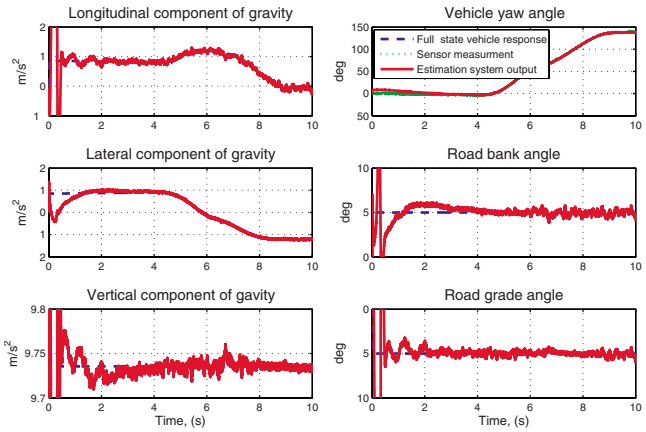

Fig. 8 Estimating road angles and their effects for Case II. The estimation system can estimate three gravitational forces and three angles accurately with the additional information of vehicle yaw angle.

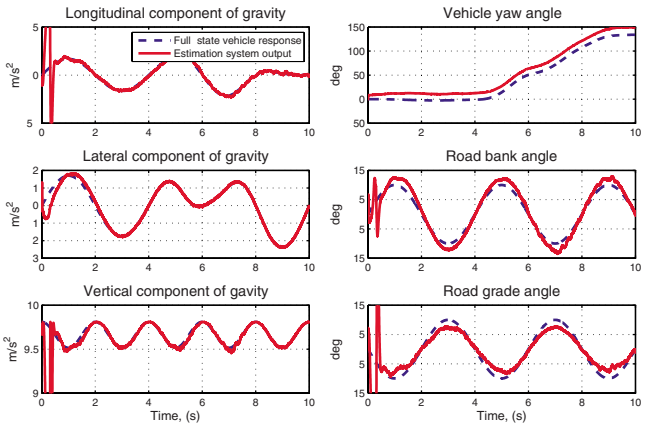

Fig. 10 Estimating road angles and their effects for Case IV. The estimation system can estimate three gravitational forces accurately when the road angles vary as sinusoidal waves.

Case III shows a vehicle moving on a road. The conditions in this case are the same as those in Case I, except that the maximum steering wheel angle is 270 deg. As shown in Fig. 9, the estimation system can obtain correct values for three gravitational forces, even when two suspensions reach their extension limits (dashed-dotted line) from 5.2 s to 6.1 s. This implies that the estimation system can still work well when two tires are off the ground. The relative accuracy of the gravitational force estimation is on average of 4.11%, 7.16%, and 0.004% for G_x^a, G_y^a, and G_z^a, respectively. The estimation accuracy in this case is worse than that in Case I. This is because the duplicated equations in Eq. (8) are removed when tires are off the ground, and that lowers the degree of observability for G_x^a, G_y^a, and G_z^a estimation.

Case IV shows a vehicle moving on a road with which the road bank angle and road grade angle are both changing with time. In this simulation, two angles are sinusoidal with the frequency of 0.25 Hz and the magnitude of 10 deg. As shown in Fig. 10, the estimation system can still obtain correct values for three gravitational forces. The relative accuracies of the gravitational force estimation are 0.92%, 5.95%, and 0.044% for G_x^a, G_y^a, and G_z^a on average. The estimation accuracy in this case is roughly the same as the case of constant angles. It can be attributed to that the fading memory techniques are in effect to optimize the performance of state convergence and estimation accuracy.

Case V shows a vehicle moving on a road. The conditions in this case are the same as those in Case IV, except that the sensor system provides three additional information: vehicle yaw rate, road bank rate, and road grade rate. These information can be obtained by attaching gyroscopes to the vehicle body. For simplicity, the standard deviations of these measurements are all assumed to be 0.01 rad/s. As shown in Fig. 11, the estimation system can obtain correct values for three gravitational forces, three angular rates, but still fails on three angles. The explanation for this case is shown in Sec. 6.

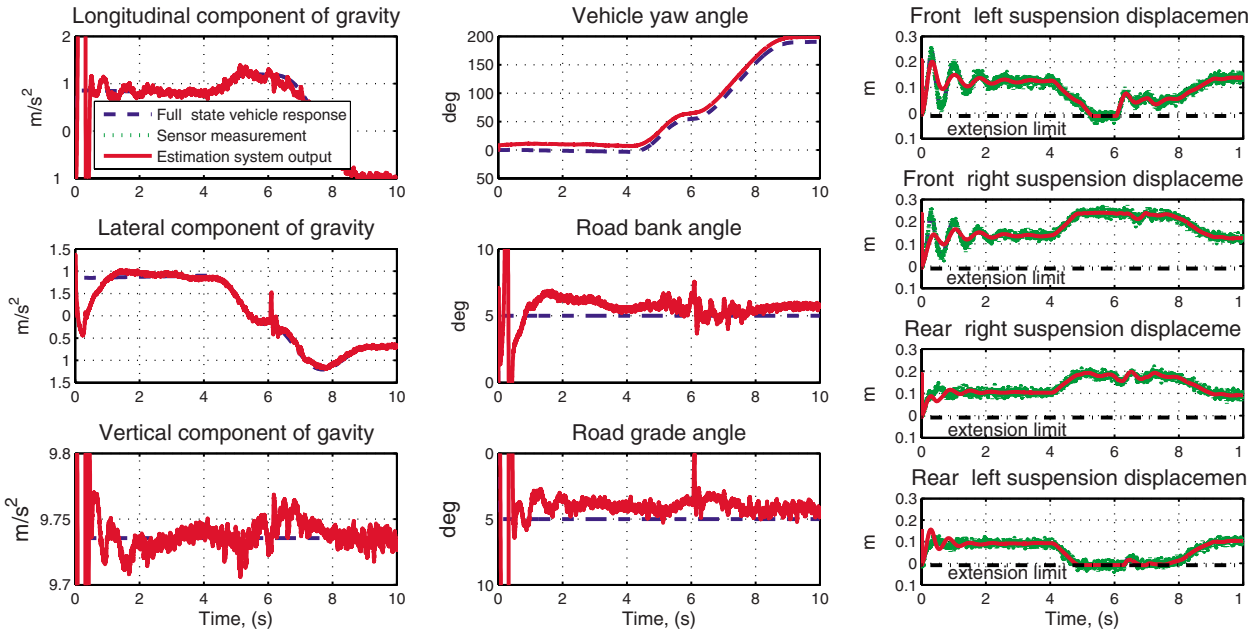

Fig. 9 Estimating road angle and their effects for Case III. The suspension displacement plots (the third column) indicate that the front-left and rear-left tires are off the ground. The estimation system can still estimate three gravitational forces accurately.

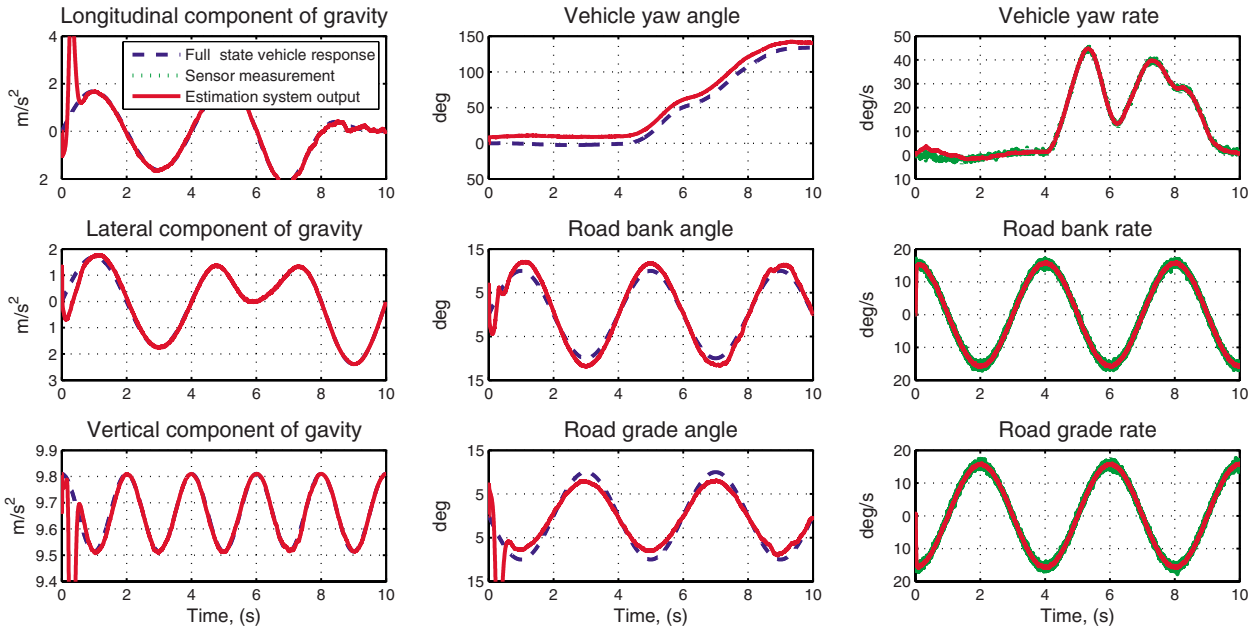

Fig. 11 Estimating road angles and their effects for Case V: With the additional sensor measurements of vehicle yaw rate, road bank rate, and road grade rate, three angle estimations still fail.

6 Discussion

Simulation results (Figs. 6 and 8) and observability analysis (Sec. 4) both indicate that three gravitational forces can be correctly estimated but three angles (θ_r, ϕ_r, ψ) cannot. Since those three angles affect vehicle dynamics only through gravitational forces and their dynamics are assumed to be static (Eq. (4)), estimating three angles is essentially the same as solving Eq. (1). According to "Wahba's problem [24]," the information of two vectors represented in both a fixed frame and a rotated frame is needed to determine three angles in a rotation matrix. In this case, only the information of gravitational forces (one vector) is available. Therefore, it is impossible to determine these angles without additional sensor measurements. However, it is interesting to note that some other approaches [4,3,8] did report successful estimations for two road angles using information of gravitational forces only. This is not because they have used better sensors/algorithms in their estimation system, but because their road bank/grade angles were defined relative to the vehicle yaw angle. It is the same situation shown in Case II, where we can obtain two road angles with a known vehicle yaw angle. However, it should be noticed that the previous definition of road angle is enough to model vehicle dynamics on a sloped road. The purpose of estimating those road angles is essentially the same as estimating the road angle effect discussed in this paper.

When trying to include additional sensors for angle determination, one would think of angular rate sensors in the first place. According to Ref. [22], the angular rate information can improve the observability of angle estimation only when the associated observability matrix does not lose rank along the entire trajectory. According to the lower plot in Fig. 7, the observability matrix of angle estimation does lose rank along the entire trajectory. Therefore, as shown in Case V, even one uses several angular rate sensors, the angle estimation is still erroneous.

This paper presents the possibility of road angle estimation even when road angles are varying with time. It would be interesting to discover the capability of the proposed method on extreme cases such as the smallest detectable road angles, the highest rates of road angles, etc. Unfortunately, because this is a nonlinear system, the estimation performance largely depends on the values of the vehicle states. Besides, due to the sinusoidal relationship between road angles and gravitational forces (Eq. (1)), a small road angle does not always lead to a small variation of gravitational forces; the frequency content of the road angles is different from that of the gravitational forces (Fig. 10). Thus, it is difficult to make a conclusive remark on these performance limits.

Due to system nonlinearity and complexity, we have not found an easy way to show the system observability analytically. Thus, the qualification of those sensors is questionable to some extent. However, the suitability of those sensors can be explained intuitively by the following: Four suspension displacement sensors provide the information of vehicle roll angle, pitch angle, and displacement/velocity/acceleration along vertical directions; the longitudinal velocity sensor provides the information of velocity/acceleration along longitudinal directions; and the lateral acceleration sensor, together with information from longitudinal velocity and tire model, provides velocity/acceleration along lateral directions. Therefore, with those three types of sensors, most vehicle states and road angle effects can be correctly estimated.

The observability analysis of the vehicle system should be performed on the original system (22-state vehicle model in this case) instead of on two subsystems (vehicle yaw model and vehicle roll model) as presented in this paper. The reason of doing observability analysis on subsystems is that our observer is constructed on these two subsystems with the switching computation scheme. According to our preliminary analysis, the observability of two subsystems is only a necessary condition for the observability of the original system. More investigations on this issue are still underway.

This paper mainly focuses on using less amounts of sensors for road angle estimations. The robustness issues from model uncertainties, such as no aerodynamics, simplified linear apart from kinematics, minimal unsprung mass dynamics, no suspension effects on tires, etc., are not fully addressed. The work for the robustness analysis is underway.

7 Conclusion

In this paper, a method for estimating road angles and their effects is presented and verified by simulation results. A 22-state vehicle model is used to ensure the estimation accuracy under various vehicle behaviors. The switching observer technique is used to suggest suitable sensors for the estimation system and to reduce the amount of equation derivations by half for the state

observer constructions. Three types of sensors are chosen to work with the estimation system, which are lateral acceleration sensor, longitudinal velocity sensor, and suspension displacement sensors. According to analysis, three components of gravitational forces can be treated as the road angle effects on the vehicle dynamics. These forces can be correctly estimated only when most of vehicle state values are known or correctly estimated simultaneously. The proposed method can estimate these forces (road angle effects) accurately under various vehicle maneuvers (for example, tires are on/off the ground) and for constant/time-varying road angles (for example, sinusoidal waves, 10 deg, 0.25 Hz). The estimation accuracy of road angle effects is less than 7.5%. On the other hand, the road angles cannot be correctly estimated neither with the current sensor deployments nor with additional angular rate sensors. They can be correctly estimated only when the vehicle yaw angle is known.

References

[1] Hsu, L.-Y., 2006, "Vehicle Rollover Prediction System Using States Observers," MA thesis, Department Mechanical Engineering, National Chiao Tung University, Hsinchu, Taiwan.

[2] Hsu, L.-Y., and Chen, T.-L., 2009, "Vehicle Full-State Estimation and Prediction System Using State Observers," IEEE Trans. Veh. Technol., **58**(6), pp. 2651–2662.

[3] Hahn, J.-O., Rajamani, R., You, S.-H., and Lee, K. I., 2004, "Real-Time Identification of Road-Bank Angle Using Differential GPS," IEEE Trans. Control Syst. Technol., **12**(4), pp. 589–599.

[4] Tseng, H. E., 2001, "Dynamic Estimation of Road Bank Angle," Veh. Syst. Dyn., **36**(4–5), pp. 307–328.

[5] Tseng, H. E., Xu, L., and Hrovat, D., 2007, "Estimation of Land Vehicle Roll and Pitch Angles," Veh. Syst. Dyn., **45**(5), pp. 433–443.

[6] Ryu, J., and Gerdes, J. C., 2004, "Estimation of Vehicle Roll and Road Bank Angle," *Proceedings of the American Control Conference*, Vol. 3, pp. 2110–2115.

[7] Ryu, J., and Gerdes, J. C., 2004, "Integrating Inertial Sensors With GPS for Vehicle Dynamics Control," ASME J. Dyn. Syst., Meas., Control, **126**(2), pp. 243–254.

[8] Jianbo, L., and Todd, A. B., 2006, "System and Method for Characterizing Vehicle Body to Road Angle for Vehicle Roll Stability Control," U.S. Patent No. 7,003,389.

[9] Bae, H. S., Ryu, J., and Gerdes, J. C., 2001, "Road Grade and Vehicle Parameter Estimation for Longitudinal Control Using GPS," *Proceedings of the IEEE on Intelligent Transportation Systems Conference*, Oakland, CA, pp. 166–171.

[10] Bar-Shalom, Y., Li, X. R., and Kirubarajan, T., 2001, *Estimation With Applications to Tracking and Navigation*, Wiley-Interscience, Hoboken, NJ.

[11] Stephen, R. P., and Gorden, L. T., 1995, "Method and Apparatus for Estimating Incline and Bank Angles of a Road," U.S. Patent No. 5,446,658.

[12] Barrho, J., Hiemer, M., Kiencke, U., and Matsunaga, T., 2005, "Estimation of Elevation Difference Based on Vehicle's Inertial Sensors," International Federation of Automatic Control.

[13] Goldstein, H., Poole, C., and Safko, J., 2002, *Classical Mechanics*, 3rd ed., Addison Wesley, New York.

[14] Toselli, A., and Widlund, O., 2005, *Domain Decomposition Methods—Algorithms and Theory*, Springer, Berlin.

[15] Tomizuka, M., Hedrick, J. K., and Pham, H., 1995, "Integrated Maneuvering Control for Automated Highway Systems Based on a Magnetic Reference/Sensing System," California Partners for Advanced Transit and Highways (PATH), Report No. UCB-ITS-PRR-95-12.

[16] Hingwe, P., 1997, "Robustness and Performance Issues in the Lateral Control of Vehicle in Automated Highway System," Ph.D. thesis, Department Mechanical Engineering, University of California, Berkeley, Berkeley, CA.

[17] Zhou, J., and Bolandhemmat, H., 2007, "Integrated INS/GPS System for an Autonomous Mobile Vehicle," International Conference on Mechatronics and Automation, pp. 694–699.

[18] Redmill, K. A., Kitajima, T., and Ozguner, U., 2001, "DGPS/INS Integrated Positioning for Control of Automated Vehicle," *Proceedings of the IEEE on Intelligent Transportation Systems*, pp. 172–178.

[19] Xia, Q., Rao, M., Ying, Y., and Shen, S. X., 1992, "A New State Estimation Algorithm—Adaptive Fading Kalman Filter," *Proceedings of the 31st Conference on Decision and Control*, Tucson, AZ, pp. 1216–1221.

[20] Hu, C., Chen, W., Chen, Y., and Liu, D., 2003, "Adaptive Kalman Filtering for Vehicle Navigation," J. Global Pos. Sys., **2**(1), pp. 42–47.

[21] Vidyasagar, M., 1993, *Nonlinear System Analysis*, Prentice-Hall, Englewood Cliffs, NJ.

[22] Kao, C.-F., and Chen, T.-L., 2008, "Design and Analysis of an Orientation Estimation System Using Coplanar Gyro-Free Inertial Measurement Unit and Magnetic Sensors," Sens. Actuators, A, **144**(2), pp. 251–262.

[23] Pallás-Areny, R., and Webster, J. G., 2001, *Sensors and Signal Conditioning*, 2nd ed., Wiley, New York.

[24] Wahba, G., 1965, "Problem 65-1: A Least Squares Estimate of Satellite Attitude," SIAM Rev., **7**(3), p. 409.